



Shahrood University of
Technology



Iranian Society of
Mining Engineering
(IRSM)

Investigation of External Work, Fracture Energy, and Fracture Toughness of Oil Well Cement Sheath using HCCD Test and CSTBD Test

Mohammad Omidimanesh, Vahab Sarfarazi*, Nima Babanouri, and Amir Rezaei¹

Mining Engineering Department, Hamedan University of Technology, Hamedan, Iran

Article Info

Received 23 January 2023

Received in Revised form 4
February 2023

Accepted 12 February 2023

Published online 12 February
2023

DOI: [10.22044/jme.2023.12633.2297](https://doi.org/10.22044/jme.2023.12633.2297)

Keywords

Hollow center cracked disc

Cracked straight through
Brazilian disc

Mode I fracture toughness

Cement slurry

Discrete element method

Abstract

This work presents the hollow center cracked disc (HCCD) test and the cracked straight through Brazilian disc (CSTBD) test of oil well cement sheath using the experimental test and Particle Flow Code in two-dimensions (PFC2D) in order to determine mode I fracture toughness of cement sheath. The tensile strength of cement sheath is 1.2 MPa. The cement sheath model is calibrated by outputs of the experimental test. Secondly, the numerical HCCD model and CSTBD model with diameter of 100 mm are prepared. The notch lengths are 10 mm, 20 mm, 30 mm, and 40 mm. The tests are performed by the loading rate of 0.018 mm/s. When the notch length in CSTBD is 40 mm, the external work is decreased 48%, related to the maximum external work of model with notch length of 10 mm (0.225 KN*mm decreased to 0.116 KN*mm). When the notch length in HCCD is 30 mm, the external work is decreased 33%, related to the maximum external work of model with notch length of 10 mm (0.06 KN*mm decreased to 0.04 KN*mm). The fracture energy is largely related to the joint length. The fracture energy is decreased by increasing the notch length. In constant to the notch length, the fracture energy of the CSTBD model is more than the HCCD model. Mode I fracture toughness is constant by increasing the notch length. The HCCD test and the CSTBD test yield a similar fracture toughness due to a similar tensile stress distribution on failure surface. The experimental outputs are in accordance to the numerical results.

1. Introduction

Cementing is an important operation in the drilling process. The cement construction in the circular space between the borehole and casing is known as cementing (Figure 1a). During the cementing operation, cement is the main material for the cementing sheath, which provides the function of suspension and protective casing (Jafariesfad et al. [1]; Cheng et al. [2]; Kremieniewski et al. [3]; Piłowska et al. [4]). Oil well cement is mostly Portland cement, with a low tensile strength, poor impact resistance, and easy cracking under the action of force (Gao et al. [5]; Wang et al. [6]; Xu et al. [7]). Furthermore, its tensile strength is also an important parameter of the stability evaluation of oil well cement. Micro-cracks of cement sheath easily appear in the cementing operation, imparting size effects, and reducing the cement strength (Xiaowei et al. [8]).

In the cementing process, numerous factors cause micro-cracks to appear in the cement sheath. During the cement slurry curing process, unhydrated cement particles and a hole exist. The mud cake attached to the wall also causes holes in the cement. Large-scale operations such as perforation and acid fracturing will result in micro-cracks in the cement (Figure 1b). The perforating operation is an important factor affecting the cement sheath strength, and the hole left by the perforation will affect the cement sheath integrity. The stress concentration around the hole causes the actual carrying capacity of the cement sheath to be lower than the designed bearing capacity (Liu et al. [9]). Ladva et al. [10] pointed out that cement sheath failure is related to the mud cake produced by the cement volume shrinkage. Scholars have mainly studied the fracture toughness of test

✉ Corresponding author: Sarfarazi@hut.ac.ir (V. Sarfarazi)

material (Dai et al. [11]; Wang et al. [12]). According to the applied stress condition, a crack propagates under the three basic failure modes or the mixed-mode condition. Mode I is the tensile opening mode, in which the crack faces separate in a direction normal to the plane of the crack. Mode

II is the in-plane sliding or shear mode, in which the crack faces are mutually sheared in the direction normal to the crack front. Mode III is the tearing or out of plane mode, in which the crack faces are sheared parallel to the crack front (Figure 2).

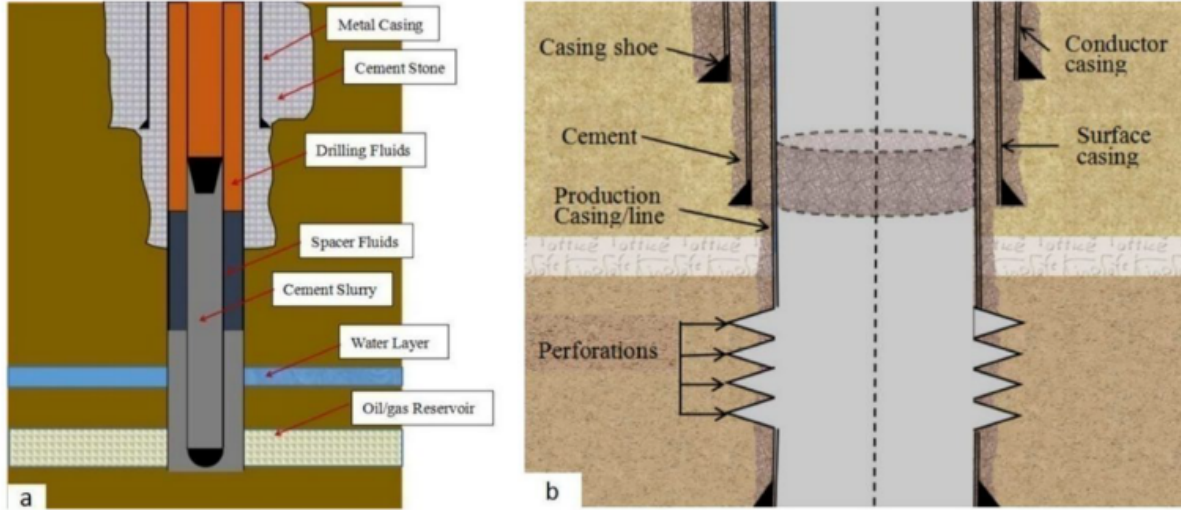


Figure 1. a) Cementing diagram, b) Perforation diagram, Xiaowei et al. [8].

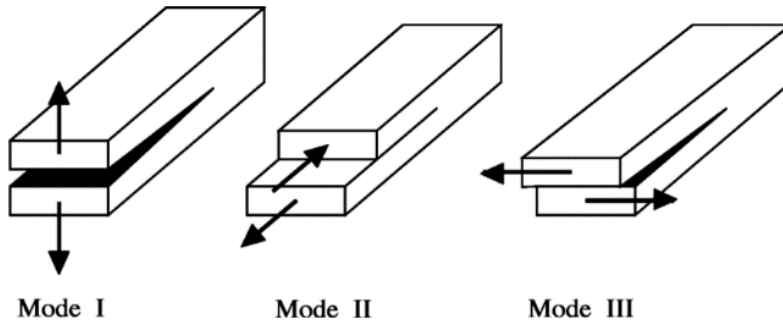


Figure 2. Three basic modes of crack propagation, Dai et al. [11].

Cement slurry failure occurred from the propagation of one or more cracks, and thus can be considered as a fracture mechanics problem. It follows that the fracture toughness of cement slurry is important in theoretical studies and engineering applications related to cement slurry failure. Among many different testing methods for rock fracture toughness, the International Society for Rock Mechanics (ISRM) suggested the chevron bend (CB), short-rod (SR) specimens, and cracked chevron-notched Brazilian disc (CCNBD) specimen. Considering specimen geometries, tensile (mode I) cracks are induced during the CB and SR tests. In addition, it has been reported that they are not appropriate for testing the fracture toughness of rock under mode II or mixed-mode cases (Fowell [13]; Lim et al., [14, 15]). Single

edge cracked round bar bend was first used by Ouchterlony [16]. Also Khan et al. [17] investigated the effect of testing method and specimen geometry such as diameter, thickness, crack length, and the type on measured fracture toughness. For this purpose, straight edge cracked round bar bend (SECRBB), semi-circular disc specimens under three point bending (SCB) and Brazilian disc specimens under diametrical compression were used. Iqbal et al. [18] selected three brittle rock types for their study, and conducted more than 200 tests to measure the values of fracture toughness. In this investigation, the chevron bend (CB) test and cracked chevron notch Brazilian disc test were used. Moreover, Tutluoglu et al. [19] conducted fracture toughness tests for different notch lengths, span lengths, and

thicknesses and diameters of the cylindrical rock specimens. Many methods including the Brazilian disc (BD) method were used for determination of mode I fracture toughness (Guo et al. [20]); Hollow center cracked disc (Awaji and Sato [21], Atkinson et al. [22], Aliha et al. [23-25]); the double-edge cracked Brazilian disc (DECBD) method (Chen et al. [26]); the flattened Brazilian disc (FBD) method (Wang and Xing [27], Keles and Tutluoglu [28]); the hollow centre cracked disc (HCCD) method (Amrollahi et al. [29]); the holed-cracked flattened Brazilian disc (HCFBD) method (Tang et al. [30]); the holed-flattened Brazilian disc (HFBD) method (Yang et al. [31]). The aim of this paper is to determine fracture parameters of oil well cement sheath and to find a relation between mode I fracture toughness and the tensile strength of cement slurry using the HCCD test and the CSTBD test by both of the experimental test and PFC2D.

2. Fracture toughness test

2.1. CSTBD test

In a circular disk with a central vertical straight notch ($\beta = 0$) subjected to a diametrical compression load (Figure 3a), the tensile cracks propagate from the notch tip. In this condition, the

following mathematical expression, proposed by Atkinson *et al.* [22], can be used for mode I fracture toughness calculation:

$$K_{IC} = \frac{2F\sqrt{a}}{\sqrt{\pi}DB} N_I \tag{1}$$

$$N_I = 1 - 4\sin^2\alpha \times (1 - \cos^2\alpha)(2a/D)^2 \tag{2}$$

2.2. HCCD test

Schematic view and geometrical dimension of HCCD specimens is presented in Figure 3b. As it can be seen in Figure 1b, HCCD is a disc with radius of R_o , in which a central hole with radius of R_i is drilled (Amrollahi et al. [29]). Two straight central cracks with length of a are created from the surface of the hole. The macro-scale mode-I fracture toughness (K_{IC}) is represented using normalized stress intensity factor (Y_I) (Figure 3c), maximum load (P), and dimension of specimen as in Equation (3).

$$K_I = \frac{P}{t(R_o - R_i)} \sqrt{\pi a} Y_I \tag{3}$$

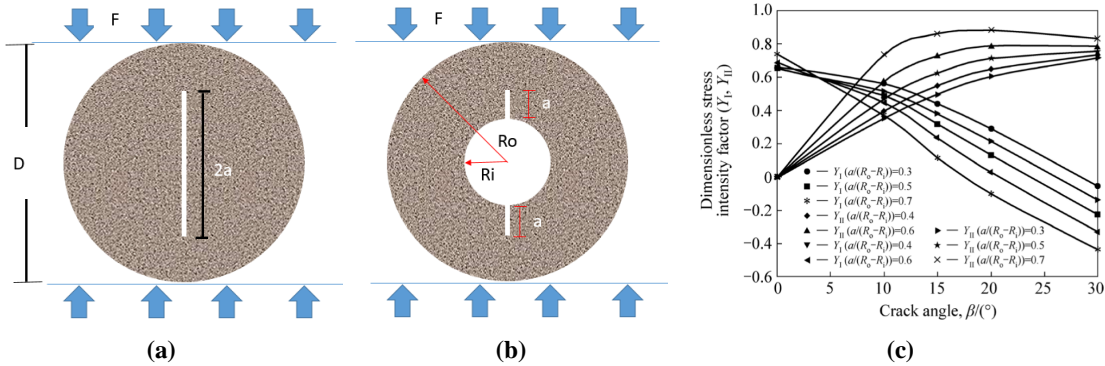


Figure 3. a) CSTBD specimen under diametrical compression (Atkinson et al. [22]), b) HCCD specimen [29], c) variations of YI with crack angle β for different crack length ratios [29].

3. Experimental Tests

Cement slurries were prepared and cured according to the standards of API Recommended Practice 10B-2.2013 [37]. The experimental formula is as follows to simulate the actual operation conditions: well cement, 2% fluid loss additive, and water with a water/cement ratio of 0.44. The fluid loss additive and cement powders were mixed and then agitated by a cement paste mixer. The cement slurry was mixed using a variable speed mixer; then it was poured into a

molds. The solidified cylindrical specimen size was 150 mm (diameter) \times 50 mm (thickness). Diameter of internal hole in the HCCD sample was 40 mm. The cement slurries were kept in standard curing molds at 60 °C with 100% relative humidity for 14 days, following which all specimens were removed from the mold. The mixing, casting, and curing of the specimens were carefully controlled to obtain reproducible specimens with precise properties. It is important to note that consistency in mixing, casting, curing, and testing was required to obtain acceptable test results. The notch lengths in both of

the CSTBD samples and HCCD samples are 1 cm, 2 cm, and 3 cm. The opening of the notch was 1 mm. Figure 4 shows the experimental set up for the CSTBD test and the HCCD test. Figure 5 and Figure 6 show the failure pattern of CSTBD

samples and HCCD samples, respectively. Totally, tensile crack was initiated from notch tip and propagated parallel to the loading axis till coalescence with sample boundary.

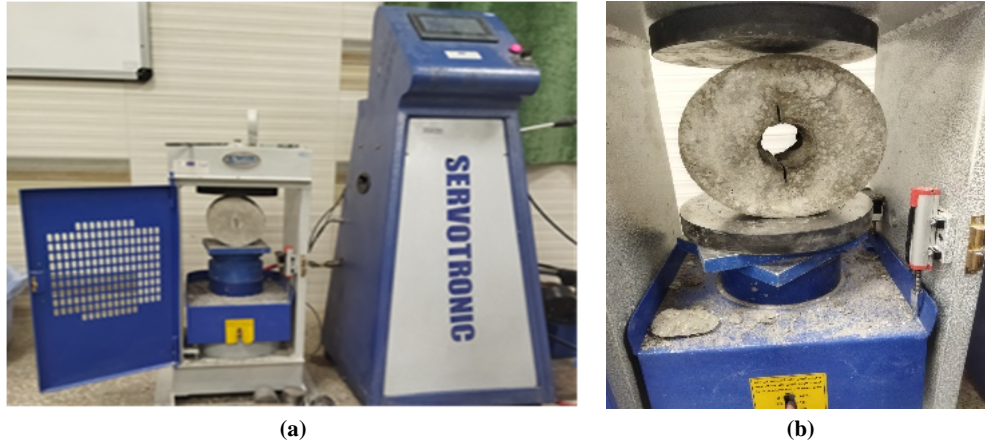


Figure 4. Experimental set up for a) CSTBD test and b) HCCD test.

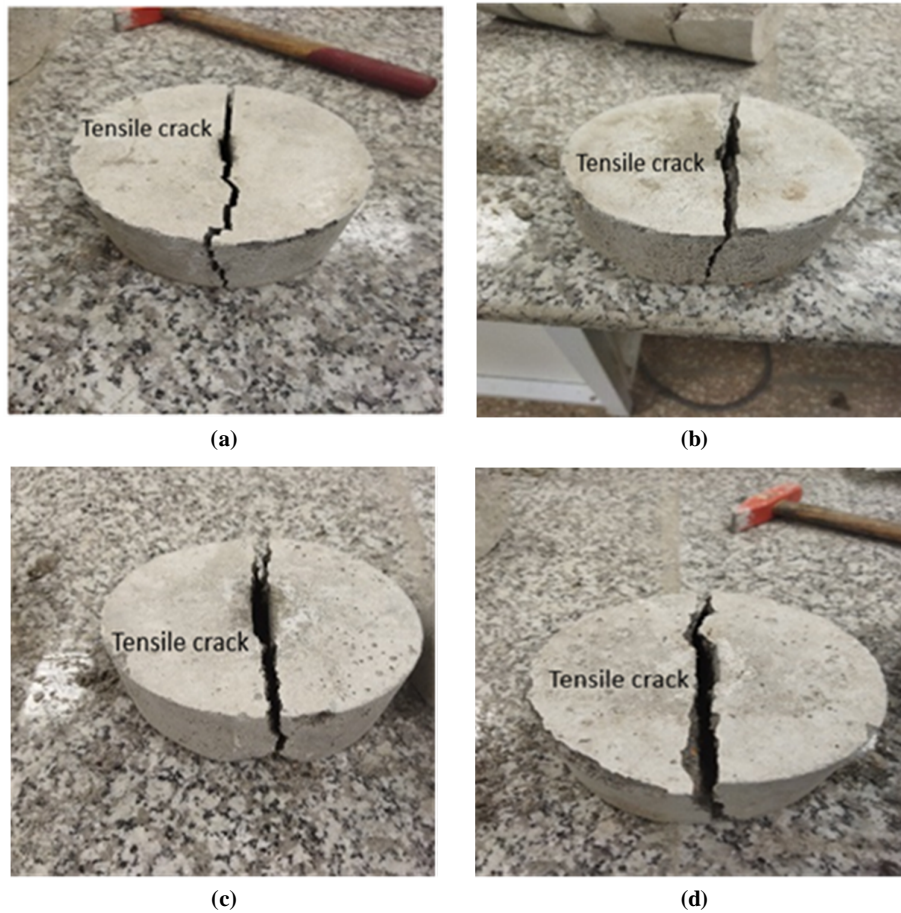


Figure 5. Failure pattern of CSTBD samples with notch length of a) 10 mm, b) 20 mm, c) 30 mm, and d) 40 mm.

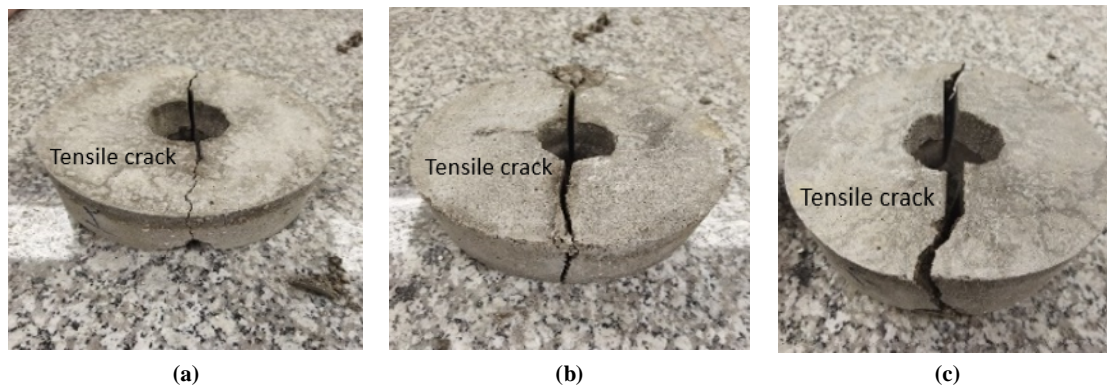


Figure 6. Failure pattern of HCCD samples with notch length of a) 10 mm, b) 20 mm, c) 30 mm.

4. Particle Flow Code

Potyondy [38] developed the flat joint (FJ) model while taking into consideration the polygonal particle grain structure. A pair of tightly connected locally flat notional surfaces that are centred at the contact point are used to represent the FJ contact. Each part has a face that acts as its imaginary surface and interacts with the faces of other parts. As a result, each facing grain looked to have a skirted, rounded or spherical core. Discs or lines make up these faces (in 2D). A group of particles connected together by FJ connections is referred to as "flat-jointed material" (FJM). The line separating facing grains discretized into elements, and these elements may or may not be joined. Once FJ is positioned at a grain-to-grain contact, the torque as well as force at each element are then reset to zero and updated in line with the force-displacement law of bond as well as the relative movement of faces. The shear force changed gradually but the normal force replaced immediately. The behaviour of the bonded element continues to be linear elastic as long as the strength does not go above its limit [39, 40].

4.1 PFC2D model preparation and calibration for cement slurry

The usual procedure for creating a PFC2D assembly is employed in this study for the construction of test models, and Potyondy [40] completely detail this procedure. Particle production, packing, isotropic stress installation (stress initialization), floating particle (floater), removal, and bond installation make up the procedure. The effects of gravity and the stress gradient caused by gravity on the macroscopic behaviour is minimal since the samples were tiny. Brazilian test calibration of particle characteristics and flat joint model was done. With the use of the micro-characteristics listed in Table 1 and standard calibration methods, a validated PFC particle assembly was produced. Figure 7 shows an experimental test results as well as a numerical simulation. The results showed a clear link between numerical simulation and experimentation. As demonstrated in Table 2, the derived specimen properties from the numerical models including the elastic modulus, Poisson's ratio, and UCS values are likewise very similar to the actual values.

Table 1. Micro-properties.

Particles		Flat joints	
Kn/ks	2	Ec (GPa)	6
Density (kg/m ³)	2400	Friction angle (°)	43
smallest disc size (mm)	0.54	Strength in tension	0.9
Maximum disc diameter (mm)	1.08	Tensile strength standard deviation (MPa)	0.09
Ec (GPa)	6	Cohesion (MPa)	9
Porosity	0.08	Cohesion standard deviation (MPa)	0.9

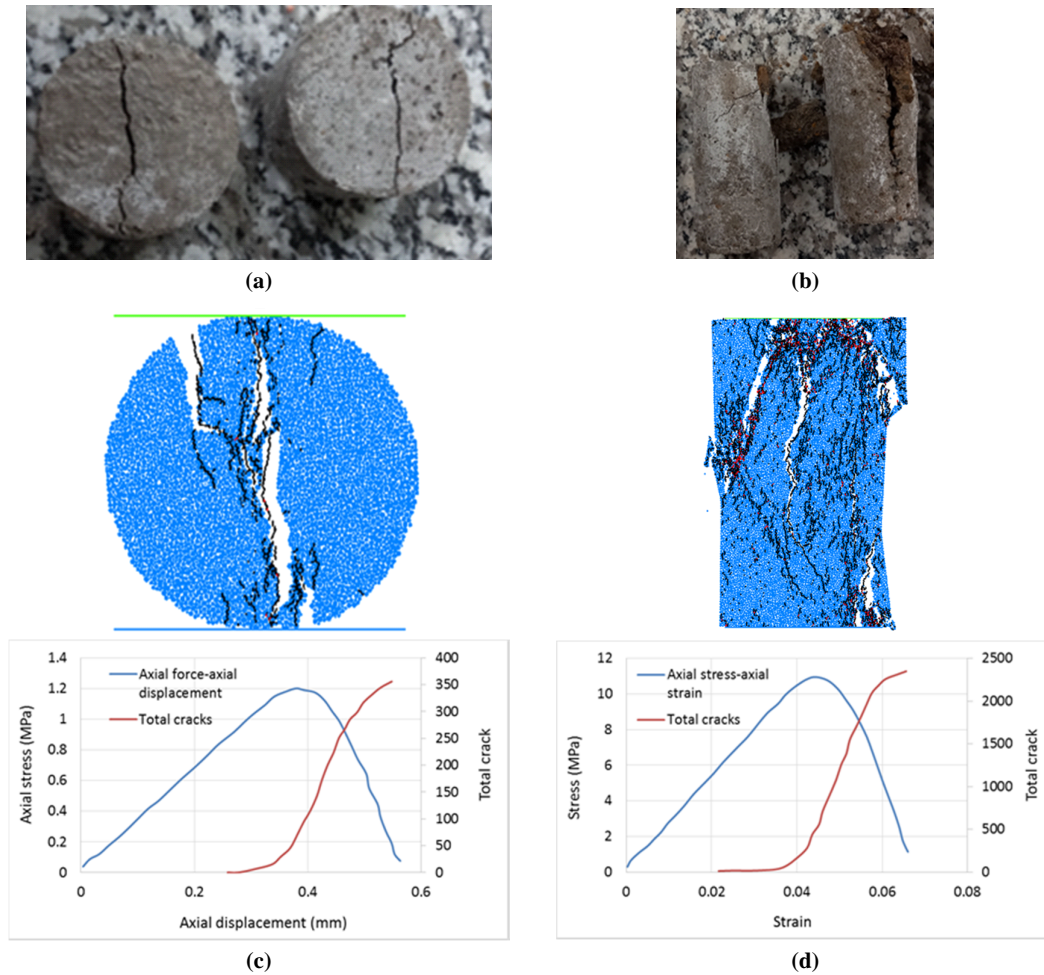


Figure 7. a) Experimental Brazilian test, b) Experimental uniaxial test, c) PFC Brazilian test, d) PFC uniaxial I test.

Table 2. Comparison of macro-mechanical characteristics between model and experiments.

Mechanical characteristics	Experimental results	PFC2D model results
Elastic modulus (GPa)	9	9.1
Poisson's ratio	0.2	0.2
UCS (MPa)	11	11.2
Brazilian tensile strength (MPa)	1.2	1.22

4.2 CSTBD test and HCCD test

The diameter of the CSTBD specimen and HCCD specimen was identically taken into account in the equivalent physical test in the numerical modelling (i.e. 150 mm). The model diameter is 150 mm. Diameter of internal hole in HCCD model was 40 mm. The notch lengths in

both of the CSTBD samples (Figure 8) and HCCD samples (Figure 9) are 1 cm, 2 cm, 3 cm, and 4 cm. The opening of the notch was 1 mm. The tests were performed by the loading rate of 0.016 mm/s. The crack initiation forces was calculated by measuring the reaction forces on the upper wall in Figure 8 and Figure 9.

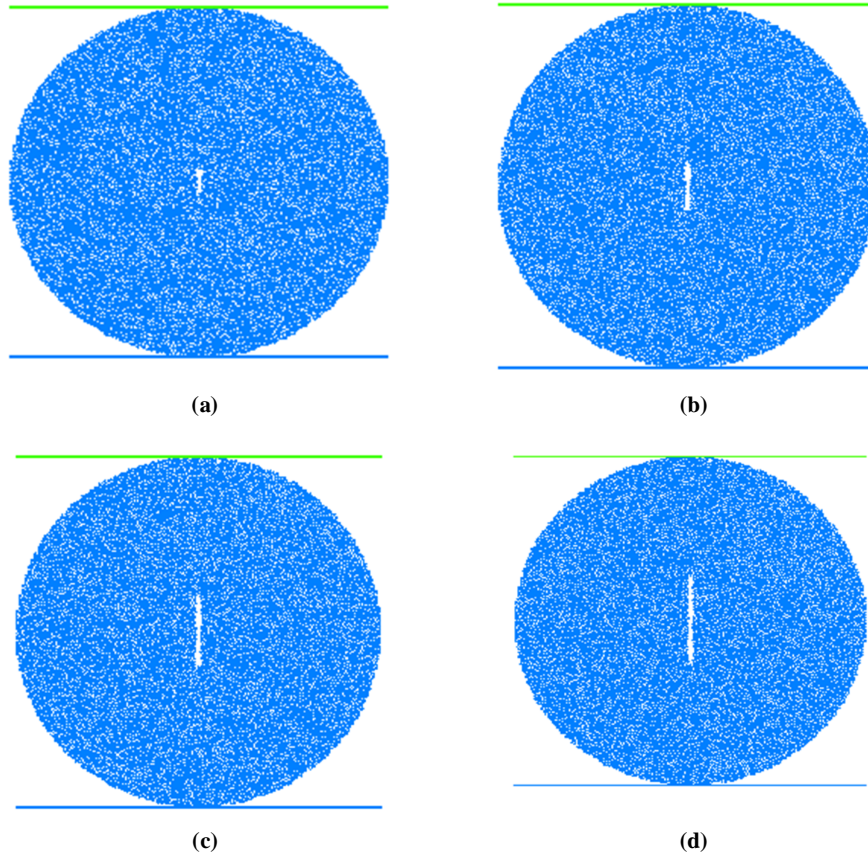


Figure 8. CSTBD samples with notch length of a) 10 mm, b) 20 mm, c) 30 mm, and d) 40 mm.

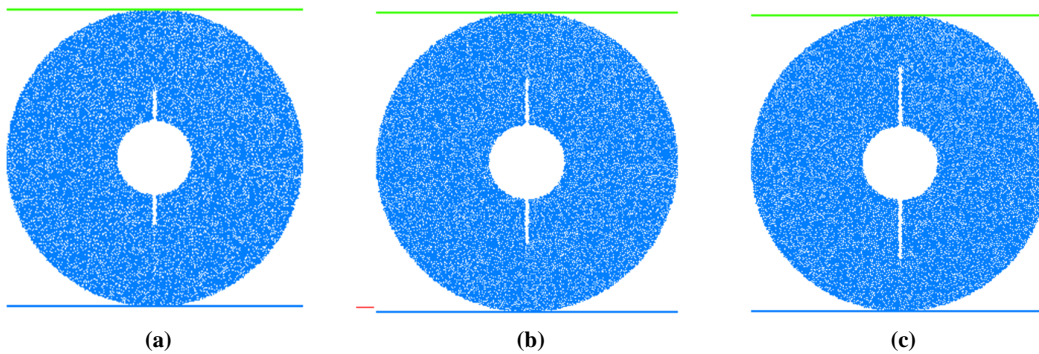


Figure 9. HCCD samples with notch length of a) 10 mm, b) 20 mm, and d) 30 mm.

5. Numerical results

5.1. Failure pattern

a) CSTBD test

Figure 10 show crack development in the CSTBD tests. Tensile cracks are shown as black lines, whereas shear cracks are shown as red lines.

The tensile fracture begins at the joint points and spreads parallel to the loading axis until coalescing at the sample edge. The similarity between Figure 10 and Figure 5 demonstrates that both the experimental samples and the computational models experience the same failure pattern.

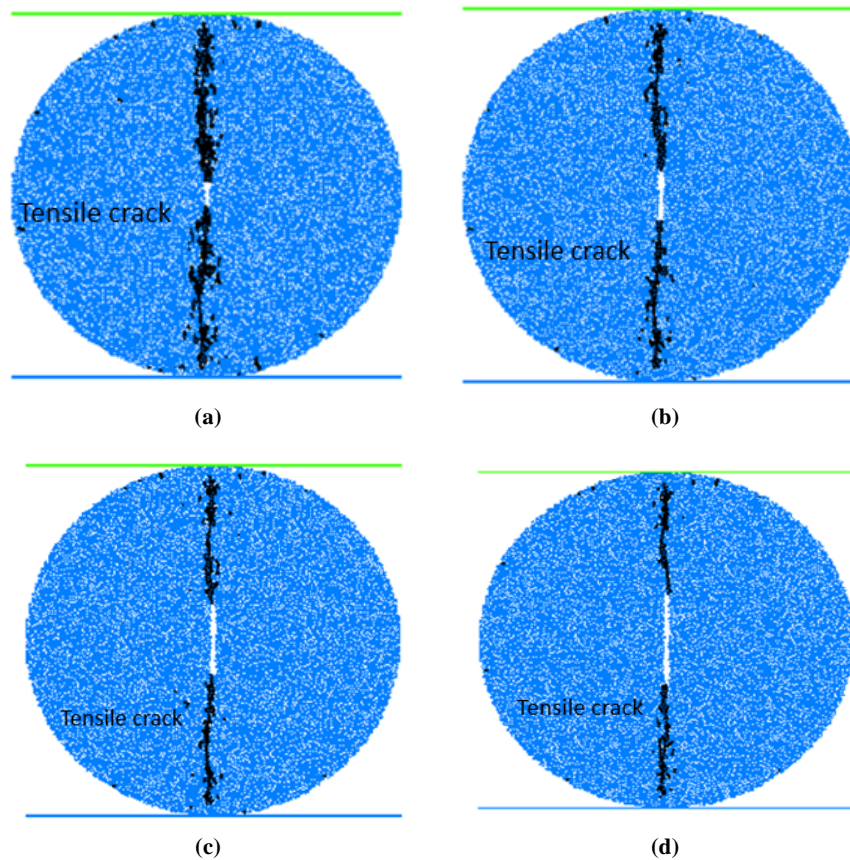


Figure 10. Failure pattern of CSTBD samples with notch length of a) 10 mm, b) 20 mm, c) 30 mm, and d) 40 mm.

b) HCCD test

Crack development in the HCCD tests is seen in Figure 11. Tensile cracks are shown as black lines, whereas shear cracks are shown as red lines. The tensile fracture begins at the notch tip and propagates parallel to the loading axis until coalescing at the sample edge. The similarity between Figures 11 and 6 demonstrates that both the experimental samples and the computational models experienced the same failure pattern.

5.2. Force-displacement curve along with total crack number

a) CSTBD test

Figure 12 shows the force-displacement curve along with the total crack number for CSTBD

models with different notch lengths. It can be seen from the figure that with the increase of force-displacement curve until the peak, the number of cracks presents three stages. In the first stage, linear part of the curve, crack number is almost zero. This is elastic stage, and there is no crack in the specimen. In the second stage, the force is near the peak load. In this stage, number of cracks is in a slowly increasing stage, which is due to continuous expansion of the notch tip. In the third stage, after the peak load, number of cracks increase rapidly, because the concrete almost enters its bearing limit and the crack propagation speed is very fast. Generally, the maximum value of number of cracks is after the peak load. Different notch lengths lead to a significant change in the cracks number.

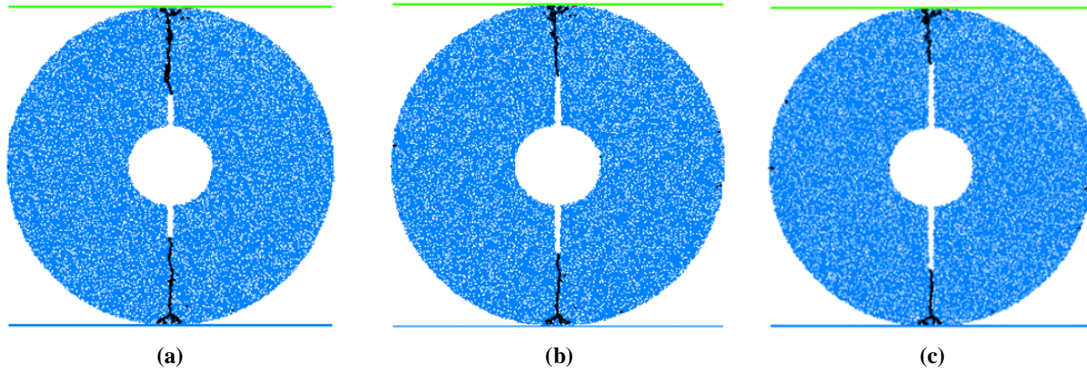


Figure 11. Failure pattern of HCCD samples a) 10 mm, b) 20 mm, and d) 30 mm.

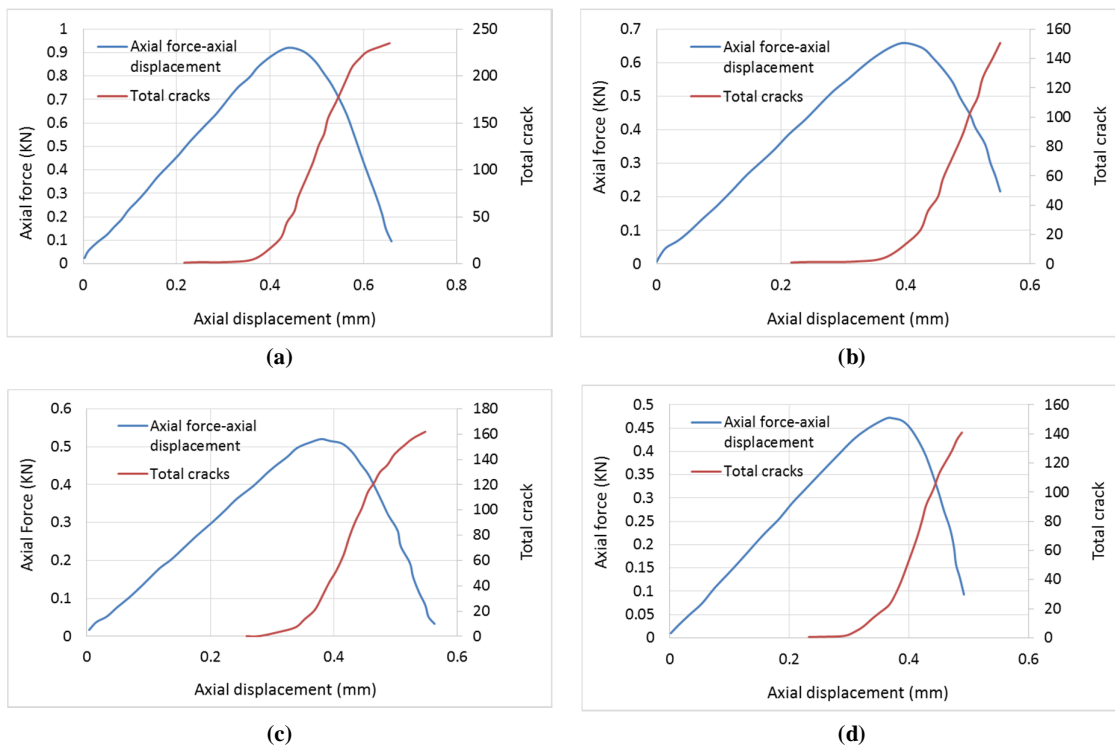


Figure 12. Force-displacement curve along with total crack number for CSTBD model containing the notch length of a) 10 mm, b) 20 mm, c) 30 mm, and d) 40 mm.

b) HCCD test

Figure 13 shows the force-displacement curve along with the total crack number for HCCD models with different notch lengths. It can be seen from the figure that with the increase of force-displacement curve until the peak, the number of cracks presents three stages. In the first stage, linear part of the curve, crack number is almost zero. This is elastic stage, and there is no crack in the specimen. In the second stage, the force is near the

peak load. In this stage, number of cracks is in a slowly increasing stage, which is due to continuous expansion of the notch tip. In the third stage, after the peak load, the number of cracks increase rapidly, because the concrete almost enters its bearing limit and the crack propagation speed is very fast. Generally, the maximum value of number of cracks is after the peak load. Different notch lengths lead to a significant change in the cracks number.

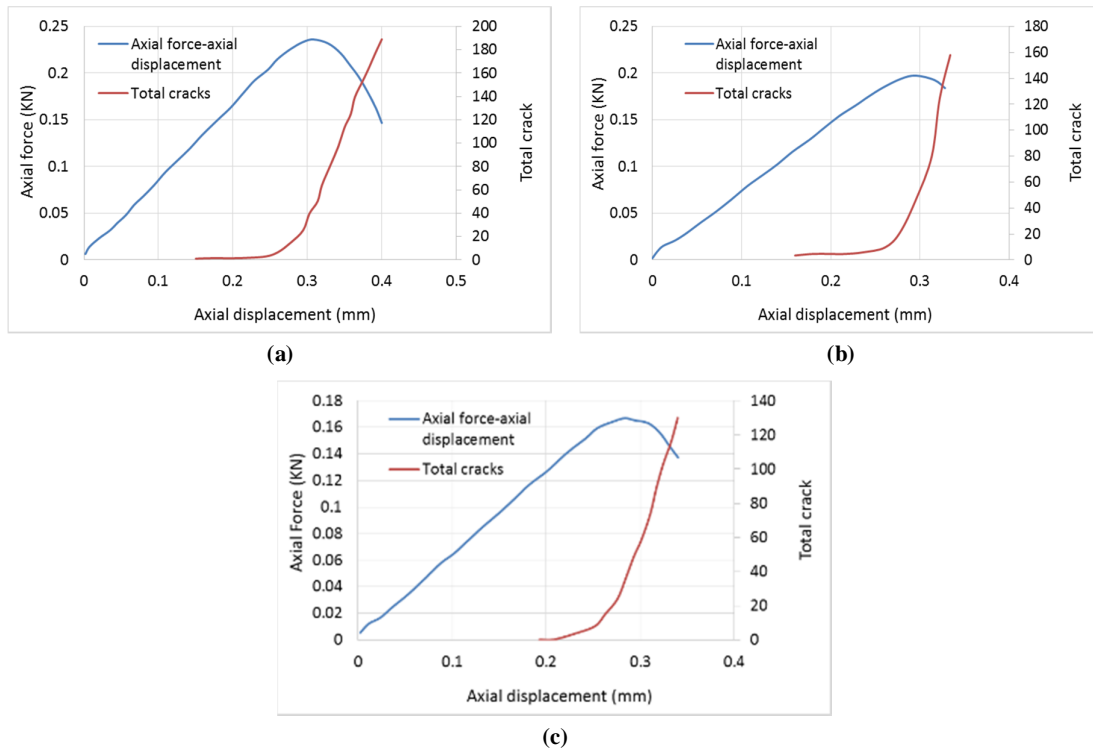


Figure 13. Force-displacement curve along with total crack number for HCCD model containing the notch length of a) 10 mm, b) 20 mm, and c) 30 mm.

5.3. Rose diagram of crack growth in CSTBD test and HCCD test

Figures 14 (a) and 14 (b) show the rose diagram of crack growth in the CSTBD test and the HCCD test, respectively. The angle between the majority of micro-cracks and vertical axis was 0° . It means that the variation of notch length and model configuration has not any influence on the crack initiation angle.

5.4. External work at peak load point in CSTBD test and HCCD test

The external work done by the loading system is illustrated by the area of the shaded region in vertical load–displacement diagram (Chen, [41]), as shown in Figure 15. The value of W that indicates external work at the final point can be calculated according to the corresponding area of the shaded region. Δ is vertical displacements at the corresponding loading points.

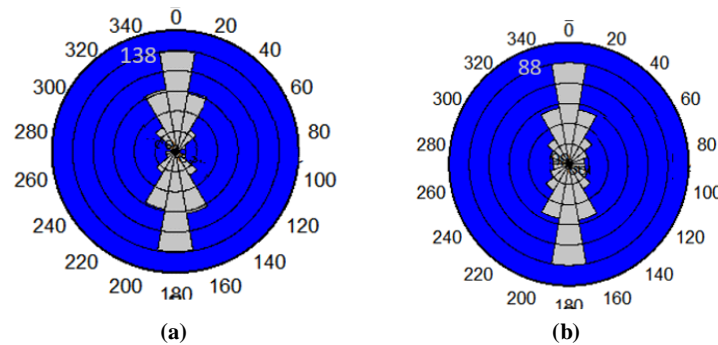


Figure 14. a) Rose diagram of crack growth for CSTBD test with notch length of 40 mm, b) rose diagram of crack growth for HCCD test with notch length of 30 mm.

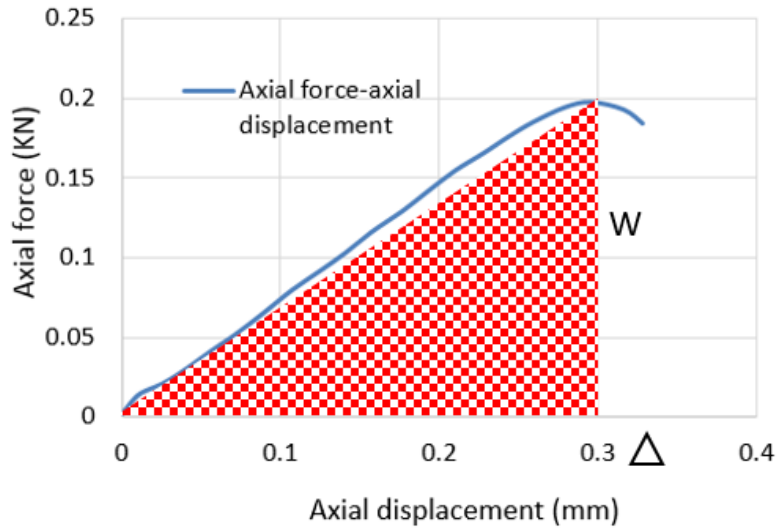


Figure 15. Load versus vertical displacement.

The variation of external works at the peak point versus the notch length for two types of specimens (CSTBD and HCCD) is shown in Figure 16. The external work is largely related to the joint length. External work was decreased by increasing the notch length. This is because the rock bridge ahead of the notch decreases when notch length increased

alongside the Y coordination systems. In constant to the notch length, the external work of the CSTBD model is more than the HCCD model. This is because the rock bridge length ahead of the notch in the CSTBD model is more than that in the HCCD model.

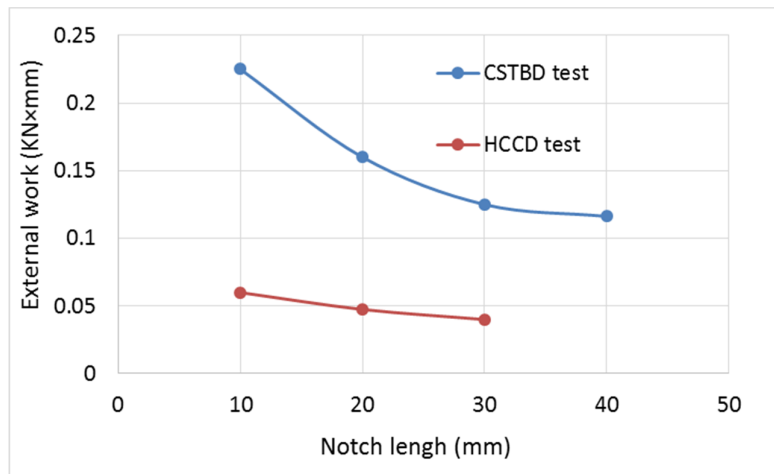


Figure 16. Variation of external work with notch length for CSTBD and HCCD models.

Table 3 shows the value of external work at pick load for different simulations. When notch length in CSTBD was 40 mm, the external work was decreased 48%, related to the maximum external work of model with notchlength of 10 mm (0.225 KN*mm decreased to 0.116 KN*mm). When notch length in HCCD was 30 mm, the external

work was decreased 33%, related to the maximum external work of model with notchlength of 10 mm (0.06 KN*mm decreased to 0.04 KN*mm).

In constant to the notch length, the external work of the CSTBD model was decreased nearly 70%, related to the external work of the HCCD model.

Table 3. External work (KN*mm) in CSTBD test and HCCD test.

	Notch length (mm)	Test configuration	
		CSTBD test	HCCD test
External work (KN.mm)	10	0.225	0.06
	20	0.16	0.0475
	30	0.125	0.04
	40	0.116	

5.5. Fracture energy in CSTBD test and HCCD test

The fracture energy, FE, can be calculated as follows (Koksal, [42]):

$$FE = (W + mg\Delta)/A \tag{4}$$

where W is the area of the region below the vertical load–displacement diagram in Figure 15, m is the mass of specimen, Δ is the maximum vertical displacement of loading position, and A = total surface area.

The variation of fracture energy versus the notch

length for two types of specimens (CSTBD and HCCD) is shown in Figure 17. The fracture energy is largely related to the joint length. Fracture energy was decreased by increasing the notch length. This is because the rock bridge ahead of the notch decreased when notch length increased alongside the Y coordination systems. In constant to the notch length, the fracture energy of the CSTBD model is more than the HCCD model. This is because the rock bridge length ahead of the notch in the CSTBD model is more than that in the HCCD model.

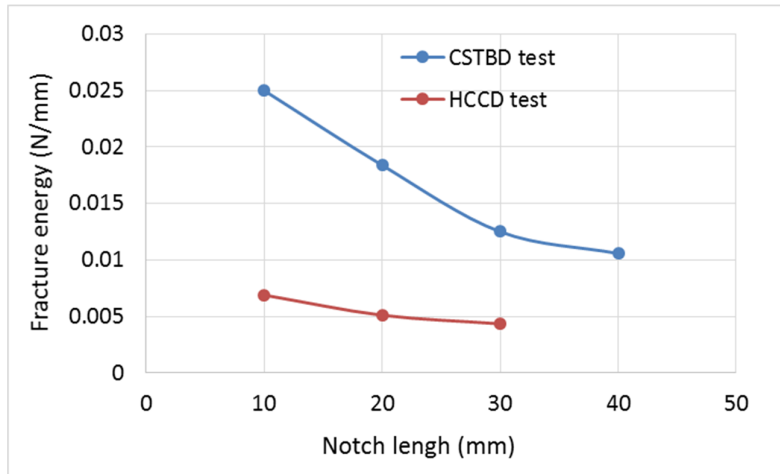


Figure 17. Variation of fracture energy with notch length for CSTBD and HCCD models.

Table 4 shows the value of fracture energy for different simulations. When notch length in CSTBD was 40 mm, the fracture energy was decreased 57%, related to the maximum fracture energy of model with notch length of 10 mm (0.025 N/m decreased to 0.0106 N/m). When notch length in HCCD was 30 mm, the fracture energy was

decreased 37%, related to the maximum fracture energy of model with notch length of 10 mm (0.06 N/m decreased to 0.04 N/m).

In constant to the notch length, the fracture energy of the CSTBD model was decreased nearly 72% related to external work of the HCCD model.

Table 4. Fracture energy (N/m) in CSTBD test and HCCD test.

	Notch length (mm)	Test condition	
		CSTBD test	HCCD test
Fracture energy (N/m)	10	0.025	0.0069
	20	0.0184	0.00511
	30	0.0125	0.00435
	40	0.0106	

5.6. Fracture toughness of CSTBD test and HCCD test

Figures 18 (a) and 18 (b) show the variation of fracture toughness with notch length for experimental test and numerical simulation, respectively. Fracture toughness of the CSTBD tests and the HCCD tests are obtained by Equation

(1) and Equation (3), respectively. Results show that Mode I fracture toughness is constant by increasing the notch length. The HCCD test and the CSTBD test yield the similar fracture toughness due to similar tensile stress distribution on failure surface. The experimental outputs and numerical results are similar.

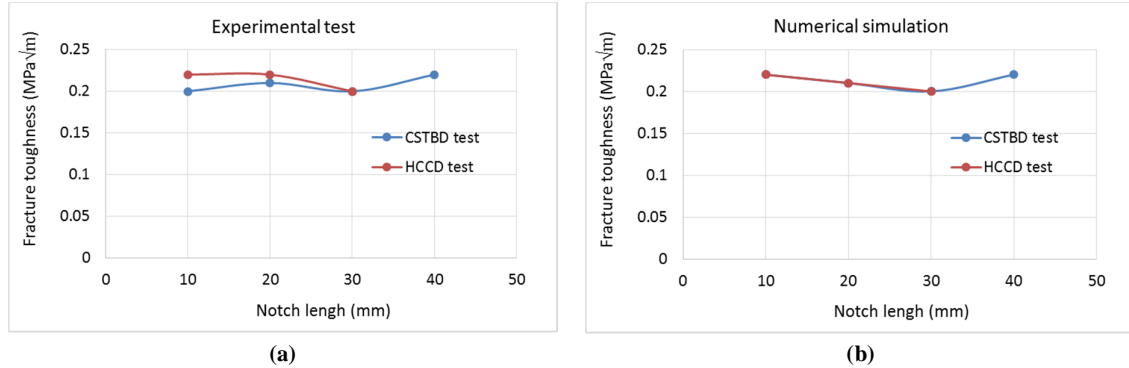


Figure 18. Variation of fracture toughness with notch length in a) experimental test and b) numerical simulation; CSTBD test and HCCD test.

5.7. Comparison between fracture toughness and tensile strength

Table 5 and Table 6 show a comparison between the fracture toughness for the CSTBD and HCCD tests in the experimental test and numerical simulation, respectively. Also Table 5 and Table 6

show the tensile strength of intact cement slurry. The results show that Mode I fracture toughness is constant by increasing the notch length. Mode I fracture toughness and tensile strength of cement slurry can be related to each other by the equation $\sigma_t = 5.8 KIC$.

Table 5. A comparison between experimental fracture toughness for CSTBD and HCCD tests.

Test method	Notch length (cm)	Fracture toughness (MPa m ^{1/2})	Tensile strength (MPa)
CSTBD	10	0.2	1.2
	20	0.21	1.2
	30	0.2	1.2
	40	0.22	1.2
HCCD	10	0.22	1.2
	20	0.22	1.2
	30	0.2	1.2

Table 6. A comparison between numerical fracture toughness for CSTBD and HCCD tests.

Test method	Notch length (mm)	Fracture toughness (MPa m ^{1/2})	Tensile strength (MPa)
CSTBD	10	0.22	1.3
	20	0.21	1.3
	30	0.2	1.3
	40	0.22	1.3
HCCD	10	0.22	1.3
	20	0.21	1.3
	30	0.2	1.3

6. Conclusion

The results show that:

- By using flat joint model, it is possible to determine the crack growth path and crack initiation stress similar to the experimental one.
- The maximum value of number of cracks is initiated after the peak load. Different notch length lead to a significant change in the cracks number.
- When notch length in CSTBD was 40 mm, the external work was decreased 48%, related to the

maximum external work of model with notch length of 10 mm (0.225 KN*mm decreased to 0.116 KN*mm). When notch length in HCCD was 30 mm, the external work was decreased 33%, related to the maximum external work of model with notch length of 10 mm (0.06 KN*mm decreased to 0.04 KN*mm).

- When notch length in CSTBD was 40 mm, the fracture energy was decreased 57%, related to the maximum fracture energy of model with notch length of 10 mm (0.025 N/m decreased to 0.0106 N/m). When notch length in HCCD was 30 mm, the fracture energy was decreased 37%, related to the maximum fracture energy of model with notch length of 10 mm (0.06 N/m decreased to 0.04 N/m). In constant to the notch length, the fracture energy of CSTBD model was decreased nearly 72%, related to the external work of the HCCD model.
- Mode I fracture toughness was constant by increasing the notch length. The HCCD test and the CSTBD test yield similar fracture toughness due to similar tensile stress distribution on failure surface.
- Mode I fracture toughness and tensile strength of cement slurry can be related to each other by the equation $\sigma_t = 5.8 KIC$.
- The experimental outputs and numerical results are similar.
- Crack propagation in the cement have a significant effect on the strength and deformation characteristics of the oil well cement. The notch position influences the cement crack initiation and direction. Fracture toughness of cement slurry is important in theoretical studies and engineering applications related to cement slurry failure. Experimentally, the measurement of fracture toughness of cement slurry is more complicated and more expensive than that of tensile strength. Therefore, the relation given here provides a helpful method for estimating the fracture toughness from the tensile strength value, which can be measured more easily. In order to investigate the reasons for the relation more deeply, a further theoretical and experimental study is necessary.

References

[1]. Jafariesfad, N. Geiker, M.R. Gong, Y. Skalle, P. Zhang, Z. and He, J.C. (2017). Cement sheath modification using nanomaterials for long-term zonal isolation of oil wells: Review. *J. Petrol Sci Eng.* 156: 662–672.

[2]. Cheng, X. Liu, K. Zhang, X. Li, Z. and Guo, X. (2018). Integrity changes of cement sheath due to contamination by drilling fluid. *Adv Cem Res.* 30: 47–55.

[3]. Kremieniewski, M. (2020). Recipe of Lightweight

Slurry with High Early Strength of the Resultant Cement Sheath. *Energies.* 13, 1583.

- [4]. Pikłowska, A. Ziąja, J. and Kremieniewski, M. (2021). Influence of the Addition of Silica Nanoparticles on the Compressive Strength of Cement Slurries under Elevated Temperature Condition. *Energies.* 4, 5493.
- [5]. Gao, C. and Wu, W. (2018). Using ESEM to analyze the microscopic property of basalt fiber reinforced asphalt concrete. *International Journal of Pavement. Research and Technology.* 11: 374–380.
- [6]. Wang, W. and Dahi Taleghani, A. (2017). Impact of hydraulic fracturing on cement sheath integrity; A modelling approach. *J. Nat Gas Sci Eng.* 44, 265–277.
- [7]. Xu, N.W. Dai, F. Wei, M.D. Xu, Y. and Zhao, T. (2015). Numerical observation of three dimensional wing-cracking of cracked chevron notched Brazilian disc rock specimen subjected to mixed mode loading. *Rock Mech Rock Eng.* 32 (2):33-44.
- [8]. Xiaowei, C. Sheng, H. Xiaoyang, G. and Wenhui, D. (2017). Crumb waste tire rubber surface modification by plasma polymerization of ethanol and its application on oil-well cement. *Appl Surf Sci.* 409: 325–342.
- [9]. Liu, T. Lin, B. and Yang, W. (2017). Mechanical behavior and failure mechanism of pre-cracked specimen under uniaxial compression. *Tectonophysics.* 32: 330–343.
- [10]. Ladva, H.K.J. Craster, B. Jones, T.G.J. Goldsmith, G. and Scott, D. (2005). The Cement-to-Formation Interface in Zonal Isolation. *SPE Drill. Completion.* 20: 186–197.
- [11]. Dai, F. Chen, R. and Xia, K. (2010) A Semi-Circular Bend Technique for Determining Dynamic Fracture Toughness. *Exp Mech.* 50: 783–791.
- [12]. Wang, P. Xu, J. Fang, X. Wen, M. Zheng, G. and Wang, P. (2017). Dynamic splitting tensile behaviors of red-sandstone subjected to repeated thermal shocks: Deterioration and micro-mechanism. *Eng. Geol.* 223,1–10.
- [13]. Fowell, R.J. (1995). Suggested method for determining mode I fracture toughness using cracked chevron notched Brazilian disk (CCNBD) specimen. *Int. J. Rock Mech. Mineral Sci. Geomech. Abstr.* 32 (1): 57–64.
- [14]. Lim, I.L. Johnston, I.W. Choi, S.K. Boland, J.N. (1994a). Fracture testing of a soft rock with semi-circular specimens under three-point bending. Part 1, 2. *Int. J. Rock Mech. Mineral Sci. Geomech. Abstr.* 31 (3): 185–212.
- [15]. Lim, I.L. Johnston, I.W. and Choi, S.K. (1994b). Assessment of mixed mode fracture toughness testing methods for rock. *Int. J. Rock Mech. Mineral Sci. Geomech. Abstr.* 31 (3): 265–272.
- [16]. Ouchterlony, F. (1981) Extension of the compliance and stress intensity formulas for the single edge crack round bar in bending, in: *Fracture Mechanics for Ceramics, Rocks, and Concrete*, ASTM International.
- [17]. Khan, K. (2000). Effect of specimen geometry and testing method on mixed mode I-II fracture toughness of a limestone rock from Saudi Arabia, *Rock mechanics and rock engineering.* 33 (3): 179-206.

- [18]. Iqbal, M. (2006). Experimental calibration of stress intensity factors of the ISRM suggested cracked chevronnotched Brazilian disc specimen used for determination of mode-I fracture toughness, *International Journal of Rock Mechanics and Mining Sciences*, 43 (8): 1270-1276.
- [19]. Tutluoglu, L. (2011). Mode I fracture toughness determination with straight notched disk bending method, *International Journal of Rock Mechanics and Mining Sciences*, 48 (8): 1248-1261.
- [20]. Guo, H. Aziz, N.I. and Schmidt, L.C. (1993). Rock fracture toughness determination by the Brazilian test. *Eng Geol.* 33 (3):177–188.
- [21]. Awaji, H. and Sato, S. (1978). Combined mode fracture toughness measurement by disk test. *J Eng Mater Technol.* 100(2):175–182.
- [22]. Atkinson, C. Smelser, R.E. and Sanchez, J. (1982). Combined mode fracture via the cracked Brazilian disk test. *Int J Fract.* 18(4):279–291.
- [23]. Aliha, M.R.M. Ayatollahi, M.R. Smith, D.J. and Pavier, M.J. (2010). Geometry and size effects on fracture trajectory in a limestone rock under mixed mode loading. *Eng Fract Mech.* 77(11): 2200–2212.
- [24]. Aliha, M.R.M. Ayatollahi, M.R. and Akbardoost, J. (2012). Typical upper bound-lower bound mixed mode fracture resistance envelopes for rock material. *Rock Mech Rock Eng.* 45 (1):65–74.
- [25]. Aliha, M.R.M. Sistaninia, M. Smith, D.J. Pavier, M.J. and Ayatollahi, M.R. (2012). Geometry effects and statistical analysis of mode I fracture in giting limestone. *Int J Rock Mech Min Sci.* 51:128–135.
- [26]. Chen, C.H. Chen, C.S. and Wu, J.H. (2008). Fracture toughness analysis on cracked ring disks of anisotropic rock. *Rock Mech Rock Eng.* 41(4):539–562.
- [27]. Wang, Q.Z. and Xing, L. (1999). Determination of fracture toughness K_{Ic} by using the flattened Brazilian disc specimen for rocks. *Eng Fract Mech.* 64 (2):193–201.
- [28]. Keles, C. and Tutluoglu, L. (2011). Investigation of proper specimen geometry for mode I fracture toughness testing with flattened Brazilian disc method. *Int J Fract.* 169 (1):61–75.
- [29]. Amrollahi, H. Baghbanan, A. and Hashemolhosseini, H. (2011). Measuring fracture toughness of crystalline marbles under modes I and II and mixed mode I-II loading conditions using CCNBD and HCCD specimens. *Int J Rock Mech Min Sci.* 48 (7):1123–1134.
- [30]. Tang, T. Bazant, Z.P. Yang, S. and Zollinger, D. (1996). Variable-notch one-size test method for fracture energy and process zone length. *Eng Fract Mech.* 55(3):383–404.
- [31]. Yang, S. Tang, T.X. Zollinger, D. and Gurjar, A. (1997). Splitting tension tests to determine rock fracture parameters by peak-load method. *Adv Cem Based Mater.* 5:18–28.
- [32]. Kulekci, G. (2021). Comparison of EFNARC and Round Plate Bending Test Methods used in Measurement of Toughness Index, Recep Tayyip Erdogan University Journal of Science and Engineering. 2(2):120-126.
- [33]. Kulekci, G., Yilmaz, A.O. and Çullu, M. (2021). Experimental Investigation of the Usability of Construction Waste as Aggregate, *Journal of Mining and Environment.* 12 (1): 63-76.
- [34]. Kulekci, G. (2021). Comparison of field and laboratory result of fiber reinforced shotcrete application. *Periodica Polytechnica Civil Engineering.* 65 (2): 463-473.
- [35]. Kulekci, G. (2019). Energy Absorption Measurement in Shotcrete by EFNARC Plaque Deflection Experiment ICADET.
- [36]. Kulekci, G. and Çullu, M. (2021). The Investigation of Mechanical Properties of Polypropylene Fiber-Reinforced Composites Produced with the use of Alternative Wastes, *Journal of Polytechnic.* 24 (3): 1171-1180
- [37]. Petroleum and Natural Gas Industries–Cements and Materials for Well Cementing. (2005). Part 1: Specification; EN ISO 10426-1.
- [38]. Potyondy, D.O. (2012). A flat-jointed bonded-particle material for hard rock. Paper presented at the 46th U.S. Rock Mechanics/Geomechanics Symposium, Chicago, USA. 55-61.
- [39]. Potyondy, D.O. (2015). The bonded-particle model as a tool for rock mechanics research and application: Current trends and future directions. *Geosystem Engineering*, 18 (1): 1–28.
- [40]. Potyondy, D.O. (2017). Simulating perforation damage with a flat-jointed bonded-particle material. Paper presented at the 51st US Rock Mechanics/Geomechanics Symposium, San Francisco, California, USA. 77-82.
- [41]. Chen, W. Konietzky, H. Tan, X. and Frruhwirt, T. (2016). Pre-failure damage analysis for brittle rocks under triaxial compression. *Computers and Geotechnics.* 74: 45-55.
- [42]. Koksall, F. (2013). Fracture energy-based optimisation of steel fibre reinforced concretes. *Engineering Fracture Mechanics.* 107: 29 –37.

مطالعه کار خارجی، انرژی شکست و چقرمگی شکست پوشش سیمانی چاه نفت با استفاده از روش های CSTBD و HCCD

محمد امیدی منش، وهاب سرفرازی*، نیما بابانوری و امیر رضایی

بخش مهندسی معدن، دانشگاه صنعتی همدان، همدان، ایران

ارسال 2023/01/23، پذیرش 2023/02/12

* نویسنده مسئول مکاتبات: sarfarazi@hut.ac.ir

چکیده:

در این مقاله، کار خارجی، انرژی شکست و چقرمگی شکست پوشش سیمانی دیوار چاه با استفاده از تست‌های دیسک حلقوی ترک‌دار و دیسک برزیلی شیاردار تعیین شد. مقاومت کششی پوشش سیمانی 1/2 مگاپاسکال است. در ابتدا با استفاده از نتایج آزمایشگاهی، مقادیر میکروپارامترهای پوشش سیمانی کالیبره شد. سپس تست‌های دیسک حلقوی ترک‌دار و دیسک برزیلی شیاردار توسط نرم افزار PFC شبیه سازی شد. قطر مدل 100 میلی‌متر و طول شکاف‌ها، 20، 30 و 40 میلی‌متر می‌باشد. نرخ بارگذاری 0,018 میلی‌متر بر ثانیه است. زمانیکه طول شکاف در آزمایش دیسک برزیلی شیاردار 40 mm است، کارخارجی 48 درصد کمتر از نمونه با طول شیار 10 mm است (0/225 KN×mm به 0/116 KN×mm کاهش می‌یابد). زمانیکه طول شکاف در دیسک حلقوی ترک‌دار 30 mm است، کارخارجی 33 درصد کمتر از نمونه با طول شیار 10 mm است (0/06 KN×mm به 0/04 KN×mm کاهش می‌یابد). انرژی شکست با طول شکاف مرتبط است. انرژی شکست با افزایش طول شکاف کاهش می‌یابد. در طول شکاف ثابت، انرژی شکست دیسک برزیلی شیاردار بیشتر از تست دیسک حلقوی ترک‌دار است. با افزایش طول شیار، چقرمگی شکست ثابت است. چقرمگی شکست در تست دیسک حلقوی ترک‌دار و دیسک برزیلی شیاردار برابر است. این مهم بدلیل توزیع تنش کششی برابر در صفحه شکست می‌باشد. نتایج عددی و آزمایشگاهی در تطابق خوبی هستند.

کلمات کلیدی: تست دیسک حلقوی ترک‌دار، دیسک برزیلی شیاردار، چقرمگی شکست، پوشش سیمانی، روش اجزا مجزا.